Available online at www.sciencedirect.com
SCIENCE DIRECT®
Journal of Solid State Chemistry 178 (2005) 1915–1924
JOURNAL OF SOLID STATE CHEMISTRY
www.elsevier.com/locate/jssc

Synthesis and electrical characterization of $Li_{0.30}Ca_{0.35}TaO_3$ perovskite synthesized via a polymerized complex route

Quoc Nghi Pham, Murugesan Vijayakumar, Claude Bohnke, Odile Bohnke*

Laboratoire des Oxydes et Fluorures (UMR 6010 CNRS), Institut de Recherche en Ingénierie Moléculaire et Matériaux Fonctionnels (FR CNRS 2575), Université du Maine, Avenue O.Messiaen, 72085 Le Mans Cedex 9, France

Received 7 February 2005; received in revised form 22 March 2005; accepted 28 March 2005
Available online 21 April 2005

Abstract

The synthesis of $Li_{0.30}Ca_{0.35}TaO_3$ perovskite by a Pechini-type polymerizable precursor method is carefully described. The thermal decomposition of the precursor and the formation of a pure perovskite phase were investigated by means of differential thermal analysis–thermogravimetric analysis (DTA–TGA) and XRD techniques. A pure and well-crystallized phase has been obtained at a lower temperature and with a much shorter synthesis time than the phase obtained by conventional solid-state reaction method. The morphology of the powder after heating at 1300 °C was observed by laser granulometry, Scanning Electron Microscopy (SEM) and Transmission Electron Microscopy (TEM). Impedance spectroscopy data allowed us to determine the electrical properties, i.e., permittivity and dc-conductivity, of the bulk and grain boundaries. The results are discussed on the assumption of the brick layer model.

Keywords: Pechini method; Citric acid; Lithium ion conductor; Perovskite; Tantalate

1. Introduction

Lithium ion-conducting materials always deserve great attention because of their potential application as solid electrolytes in electrochemical devices such as high-energy batteries. The compounds of the solid solution $Li_{3x}La_{2/3-x}TiO_3$ are well known to be one of the best lithium ionic conductors (10^{-3} S cm^{-1} at room temperature for $x = 0.11$) [1,2]. However, they are chemically unstable against Li metal, because of the thermodynamically possible Ti^{4+} reduction. This precludes their use in high-density lithium battery with Li metal as anode with a direct contact between the anode and the electrolyte. Apart from lithium batteries application, Bohnké et al. recently reported the use of these perovskite titanate ceramics as ion-selective electrodes for pH detection [3,4]. In search of a more stable *B*-site cation than Ti in the perovskite lattice, Ta was found to be less reducible and more appropriate [5–8]. We recently showed that the $Li_{2x}Ca_{0.5-x}TaO_3$ perovskite compounds can be obtained, by means of the conventional Solid-State Reaction (SSR) method, after heating at very high temperature (1500 °C) and for a long time (30 h) with several intermediate grindings. The quenching of the pellets in air to room temperature is essential to obtain a pure perovskite phase. These compounds belong to a solid solution that exists for $0.05 \leqslant x \leqslant 0.25$, the unit cell exhibits an orthorhombic distortion of the cubic perovskite model (s.g. *Pnma*) and shows a maximum dc-conductivity of 2×10^{-6} S cm^{-1} at 200 °C for $x = 0.10$ [9,10].

In order to find an easier and more appropriate way to prepare these compounds for industrial application, we investigated the Pechini route. This process is well-known to be a versatile technique to obtain fine, homogenous powders of oxide at low temperature and with short time. However, the difficulty encountered in

*Corresponding author. Fax: +33 2 43 83 35 06.
E-mail address: odile.bohnke@univ-lemans.fr (O. Bohnke).

0022-4596/$ - see front matter © 2005 Elsevier Inc. All rights reserved.
doi:10.1016/j.jssc.2005.03.043

this synthesis route is to find compatible and stable precursors. Generally, alkoxide precursors are used but they are extremely sensitive to moisture and has to be processed under a strictly dry atmosphere. To avoid the use of alkoxide compounds as starting reagents, we used a Pechini-type Polymerized-Complex (PC) route. This kind of chemical synthesis, based on high viscosity polyesters obtained from citric acid—metal chelates and polyhydroxyl alcohols, was first developed by Pechini [11]. Szanics et al. proposed a modified PC method, that they successfully used to synthesize $LiTaO_3$ from a methanol–citric acid solution of $TaCl_5$ as precursor, without any special care about moisture in air [12].

In the present investigation, we describe the synthesis of $Li_{0.30}Ca_{0.35}TaO_3$ by using this modified PC method. The advantages of this chemical solution method is discussed in comparison to the classical SSR technique. Thermal analysis is performed on the powder precursor and the phase evolution with firing temperature, from 500 to 1300 °C, is studied by X-ray diffraction (XRD). The morphology of the resulting $Li_{0.30}Ca_{0.35}TaO_3$ ceramic is characterized by scanning and transmission electron microscopy and laser granulometry. Finally, the electrical conductivity of Ca-tantalate pellets are measured, the influence of the synthesis method on the grain boundaries properties are discussed.

2. Experimental

$TaCl_5$ (99.8%), Li_2CO_3 (99.997%) from Aldrich and $CaCO_3$ (99.0%) from Merck were used as starting materials. The traces of water and adsorbed gases were removed from $CaCO_3$ and Li_2CO_3 by keeping these compounds in an oven at 110 °C before weighting. The polymer precursor was prepared from the solution of the above reagents with citric acid (CA) (99.5%) from Riedel-de Haën in methanol (99.8% Merck) and ethylene glycol (EG) (99%) from Aldrich. The detailed procedure used for the synthesis is given in the next part of the paper.

Thermogravimetric analysis (TGA) and differential thermal analysis (DTA) were simultaneously performed with a Setaram TGDTA92 equipment, with a heating rate of 5 °C min^{-1} in air using Pt crucibles.

Powder XRD patterns of the fired powder precursor have been recorded at room temperature with a Siemens D500 (Cu$K\alpha$ radiation) in the 2θ range from 5° to 90°. A slow scan pattern of the final $Li_{0.30}Ca_{0.35}TaO_3$ powder was recorded with a Philips X'Pert PRO diffractometer (Co source) equipped with a X'celerator detector, in the 2θ range from 5° to 125° with an interpolated step of 0.0167°. This pattern was analysed through the Rietveld method with the FULLPROF software [13].

Microstructure observations were performed using a Hitachi 2300 Scanning Electron Microscope (SEM) with Au-sputtered samples. Thin specimens for Transmission Electron Microscopy (TEM) study were obtained by ultrasonically dispersing particles in ethanol and deposing one drop of the resulting suspension on a Cu grid covered with a holey carbon film. After drying, the grid was fixed in a side-entry $\pm 30°$ double-tilt specimen holder and introduced in a JEOL-2010 electron microscope operating at 200 kV.

Particles size was determined using a Beckman-Coulter LS 230 equipment in water at room temperature. This equipment uses a 5 mW, 750 nm laser beam and 126 detectors placed at a range of angles up to 35° to the laser beam. Conventional (Fraunhöfer) laser diffraction is used to measure particles in the size range from 2 mm to 0.4 μm. A second unit measures particle size down to 0.04 μm using a technique that Coulter refers to as PIDS (Polarizations Intensity Differential Scatter). This is also based on laser diffraction, but this unit measures light flux only at high angles to the beam. Using six detectors and a tungsten light source, the PIDS unit compares the intensity of the scattered light at two polarization angles and at three different wavelengths (450, 600 and 900 nm), allowing measurements down to 0.04 μm. In order to separate the soft agglomerates, in situ ultrasonic vibration has been used before measurement of the particles size.

Electrical conductivity measurements have been carried out by impedance spectroscopy on pellets of $\varnothing \approx 4.25$ mm in diameter and $L \approx 1.25$ mm in thickness with ion-blocking sputtered Pt electrodes under dehydrated N_2 atmosphere in a two-probe cell (Data Line). The Frequency Response Analyser (Solartron 1260) and the Dielectric Interface (Solartron 1296) were used in the frequency domain from 5 MHz to 0.1 Hz and in the temperature range from 75 to 300 °C. The procedure used for data acquisition and data analysis were described previously [10]. We have to note that the data-modulus type of data weighting has been used for diagrams refinement [14].

3. Results and discussion

3.1. Synthesis and firing of the powder precursors

Fig. 1 shows the flow chart describing the synthesis procedure used to prepare $Li_{0.30}Ca_{0.35}TaO_3$. $TaCl_5$ was chosen as a source of tantalum, which is much less expensive and more stable than Ta-alkoxides. In a typical synthesis of 1 g of $Li_{0.30}Ca_{0.35}TaO_3$, 21 mL of methanol (16.59 g) was used as a solvent to dissolve 0.00408 mol of $TaCl_5$ (1.4617 g). A large excess of CA (0.1 mol = 19.2 g), which corresponds to a CA/Ta = 100:4 ratio, was added to the $TaCl_5$-methanol solution to chelate the metal cations. This step is carried out in a glove box in order to avoid hydrolysis of $TaCl_5$.

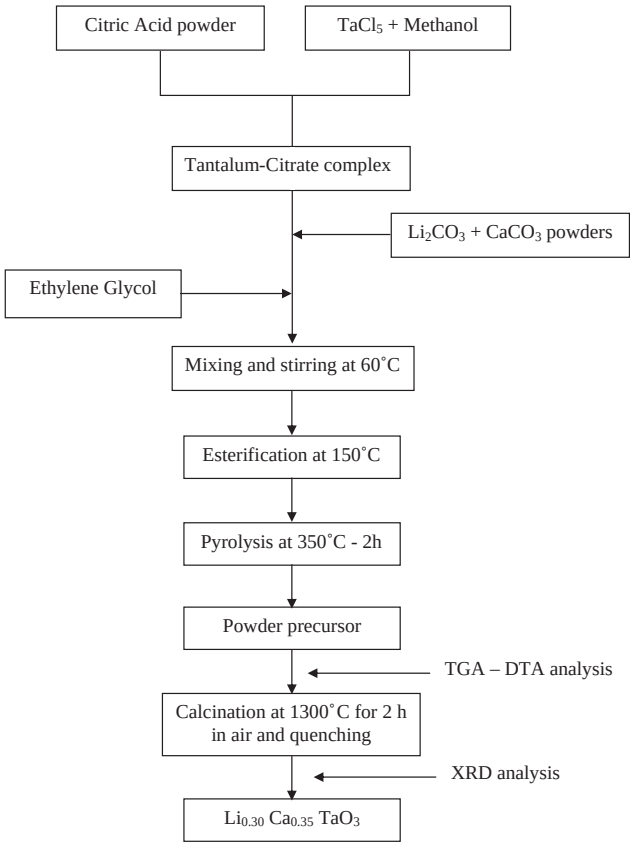

Fig. 1. Flow chart for preparation of $Li_{0.30}Ca_{0.35}TaO_3$ by Polymerized Complex method.

The solution is then taken out from the glove box. 0.00061 mol of Li_2CO_3 (0.0452 g) and 0.00143 mol of $CaCO_3$ (0.1429 g) were added and the mixture was magnetically stirred for 1 h producing a transparent solution of CA-metals chelates. Subsequently, 0.4 mol of EG (22.3 mL = 24.8 g) was added to this solution that becomes reddish in colour. The CA/EG molar ratio was taken as 1:4. This ratio ensures a large excess of hydroxyl groups to promote the formation of low molecular weight oligomers. All the procedures described above were carried out at room temperature. The clear solution thus prepared was heated at ~60 °C for 2 h under stirring to remove most of the methanol. The temperature is then increased to 150 °C to promote esterification between the hydroxyl groups of EG and the carboxylic acid groups of CA and polymerization. The prolonged heating at ~150 °C produced a viscous, bubbly mass that formed a yellow transparent glassy resin upon cooling. No visible formation of precipitation or turbidity was observed during the polymerization. It can be assumed that the polymer precursor contains lithium, calcium and tantalum cations trapped homogeneously throughout the polymer matrix. This configuration favours the synthesis of an homogeneous oxide at temperature lower than the one used for solid-state reaction. Therefore, pyrolysis of the polymer is performed at 350 °C for 2 h in a furnace that yields a black powder precursor, called hereafter "powder precursor". The black colour indicates that the powder contains carbon.

In order to determine the firing temperature of the powder precursor, TGA and DTA are performed on this black powder precursor. Fig. 2 illustrates the resulting curves obtained from the powder precursor fired in air, with a heating rate of 5 °C min^{-1}, in the temperature range from 30 to 1350 °C. The TGA plot indicates a small weight loss of ~3% up to 150 °C, an abrupt weight loss of ~51% in the temperature range from 300 to 500 °C and no further weight loss up to 1350 °C. The first weight loss is attributed to the removal of water and methanol molecules adsorbed on the sample particles surface. The second abrupt weight loss associated with exothermic DTA peak is due to the degradation of the polymer, converting the organic component into CO_2 and H_2O. At higher temperatures (600–1350 °C) the chemical reactions between the precursors occur. These chemical reactions do not lead to weight loss, as shown in the TGA plot. According to these curves, the powder precursor is fired in open air for 2 h, at temperature between 500 and 1300 °C, with a heating rate of 5 °C min^{-1}.

Figs. 3a–f show the XRD patterns of powders obtained after firing the powder precursor in air at different temperatures for 2 h with a heating rate of 5 °C min^{-1} and natural cooling. The starting powder precursor, when heat-treated below 500 °C, is amorphous in nature (not shown here). Its grey colour indicates the presence of residual carbon. When heat-treated at 500 °C (3*a*) and above, the powder appears slightly yellowish in colour, which suggests the complete burnout of residual carbon from the precursor powder. At 700 °C (3*c*), the two well-known phases $LiTaO_3$ and $CaTa_2O_6$ (rynersonite) are observed and these phases are considered to be intermediate phases. The formation of the crystalline perovskite phase has been only observed on the XRD pattern at 1200 °C (3*f*) along

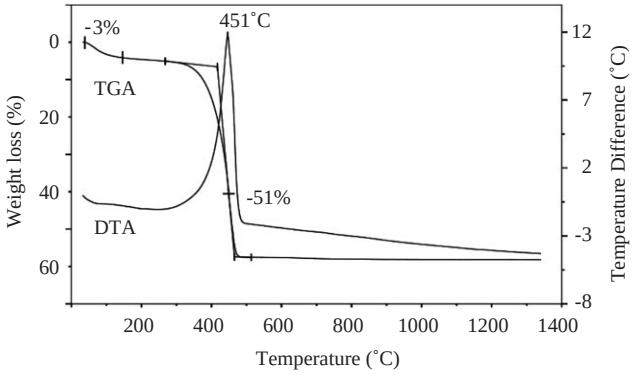

Fig. 2. TGA and DTA curves of powder precursor in air with a heating rate of 5 °C min^{-1}.

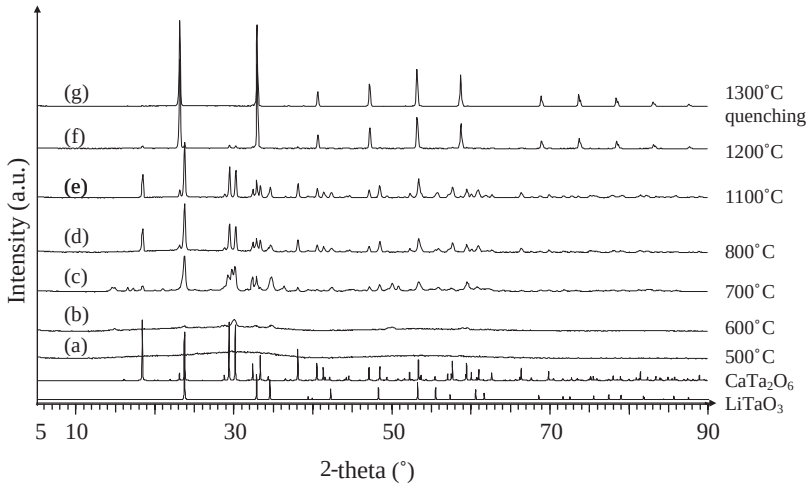

Fig. 3. XRD patterns of the "powder precursor" after calcination in air for 2 h at different temperatures. Patterns (a)–(f) have been obtained at room temperature for samples heated and slowly cooled. Pattern (g) has been obtained for a sample heated at 1300 °C for 2 h and quenched to room temperature.

with intermediate phases mentioned above. The increase of the heat treatment time from 2 to 4 h or the quenching of the powder at this temperature (1200 °C) have been carried out, however both failed to eliminate the intermediate phases. A further increase of temperature up to 1300 °C followed by quenching to room temperature (3*g*) results in the desired pure perovskite phase without any intermediate and impurity phases. As described in our previous paper [9], the quenching enables us to avoid the formation of the two intermediate phases that were present at lower temperature. These results indicates the existence of a reversible reaction between the above two intermediate phases and the perovskite phase. The pure perovskite phase, formed at 1300 °C, tends to dissociate into the intermediate phases ($LiTaO_3$, $CaTa_2O_6$) during a slow cooling of the samples, according to the following equilibrium:

$$0.30LiTaO_3 + 0.35CaTa_2O_6 \rightleftharpoons Li_{0.30}Ca_{0.35}TaO_3$$

In order to avoid this dissociation and to form a pure perovskite phase, the samples have to be quenched to room temperature.

3.2. Characterization of the quenched tantalate

3.2.1. Microstructure

Fig. 4 presents a XRD pattern (slow scan) of the final ceramic obtained after firing the powder precursor at 1300 °C for 2 h and quenching in air to room temperature, as described above. According to our previous structural study on the series $Li_{2x}Ca_{0.5-x}TaO_3$ obtained by SSR [9], we used the same procedure to analyse the pattern and found that all the peaks of the XRD pattern of this $Li_{0.30}Ca_{0.35}TaO_3$ phase can be indexed in the same orthorhombic *Pnma* (No. 62) space group, indicating the formation of a single phase, identical to

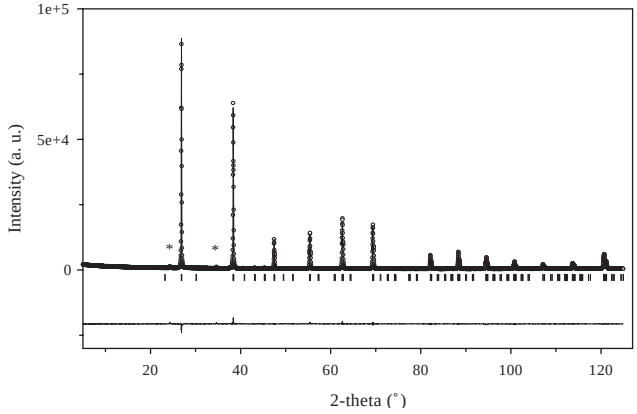

Fig. 4. Observed (…) and calculated (–) powder XRD patterns of $Li_{0.30}Ca_{0.35}TaO_3$ sample after calcination at 1300 °C for 2 h and quenching. The difference pattern is shown below at the same scale, the vertical bars are related to the calculated Bragg reflection positions. The asterisks (*) refer to K_β of Co. The cell parameters are: $a = 5.4427(6)$ Å, $b = 7.7110(3)$ Å, $c = 5.4456(6)$ Å.

the phase obtained by the classical SSR method. This analysis confirms that the material prepared by the PC route has the same crystallographic characteristic as the one prepared by solid-state reaction.

The SEM micrographs of $Li_{0.30}Ca_{0.35}TaO_3$ after calcination (Fig. 5) reveal the microstructure of the ceramic sample. After heating at 1300 °C for 2 h, the ceramic is made of small grains of diameter smaller than 1 μm (Fig. 5a). However these grains agglomerate as shown in Fig. 5b. This is clearly revealed by laser granulometry, as shown in Fig. 6, the solid line indicates the percentage of grains for a particular diameter, shown in the *X*-axis, whereas the dashed line corresponds to the percentage of volume occupied by the grains with a size smaller or equal to the considered one. This histogram has been obtained from the same

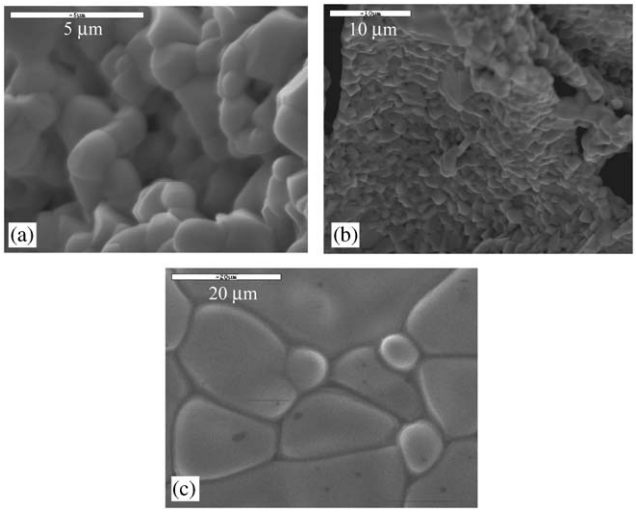

Fig. 5. SEM micrographs of sample obtained by PC route after heating at 1300 °C for 2 h and quenching (a, b) and obtained by SSR (c).

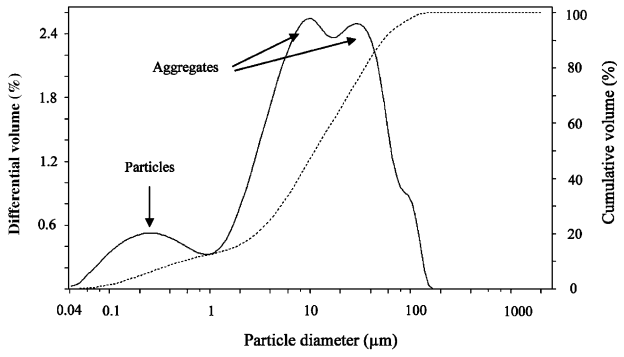

Fig. 6. Histogram of the particles and aggregates size of $Li_{0.30}Ca_{0.35}TaO_3$ sample. Differential (solid line) and cumulative (dashed line) volume percentage particle size distribution are plotted on the left and the right axis, respectively.

$Li_{0.30}Ca_{0.35}TaO_3$ powder as used for SEM experiments. The powder has been ultrasonically treated in situ in water for 1 min with a power of 20 W. The presence of three well-defined peaks shows that most of the grains are aggregated. The grain size is centred around 0.2 μm and the aggregate sizes are centred around 8 μm for one and around 35 μm for the second one. The $Li_{0.30}Ca_{0.35}TaO_3$ powder obtained by this technique presents smaller grains, even after heat-treatment at 1300 °C for 2 h, than those obtained by the conventional solid-state reaction after heat-treatment at higher temperature (1500 °C) for longer time (30 h), as shown in Fig. 5c. It is clearly observed that the synthesis route influences the microstructure of the material as well as the grain size. The average grain size of the tantalate obtained by PC route is around 0.2 μm, these grains agglomerate to form big aggregates of average size around 20 μm. The oxide prepared by SSR method shows grains around 10 μm size which also agglomerate in 10–100 μm aggregates [10]. It is worth noting that SEM micrographs (Figs. 5b and c) show that the grain boundaries are always smaller than the grain size whatever the synthesis procedure used. We will show, in the remaining part of this paper, in what extend the microstructure influences the total impedance of the ceramic.

To probe the crystallinity of the oxide TEM experiments have been performed. The micrographs are identical to the one previously obtained with tantalates synthesized by SSR, confirming that the oxide, prepared by PC route, is well-crystallized despite the lower synthesis temperature and time used. These micrographs also showed the same "mosaic" structure [9].

3.2.2. Electrical properties

First, it has to be noted that the conductivity in these samples is mostly ionic in nature since we did not detect any electronic conductivity. Fig. 7 shows typical impedance diagrams, recorded at 200 °C under dry N_2 atmosphere, of the tantalates obtained by the PC route (a) and the classical SSR (b). To be compared, the plots have been normalized to the geometric factor of the samples. It can be observed, in Fig. 7, that the total resistance of the sample (bulk and grain boundaries)

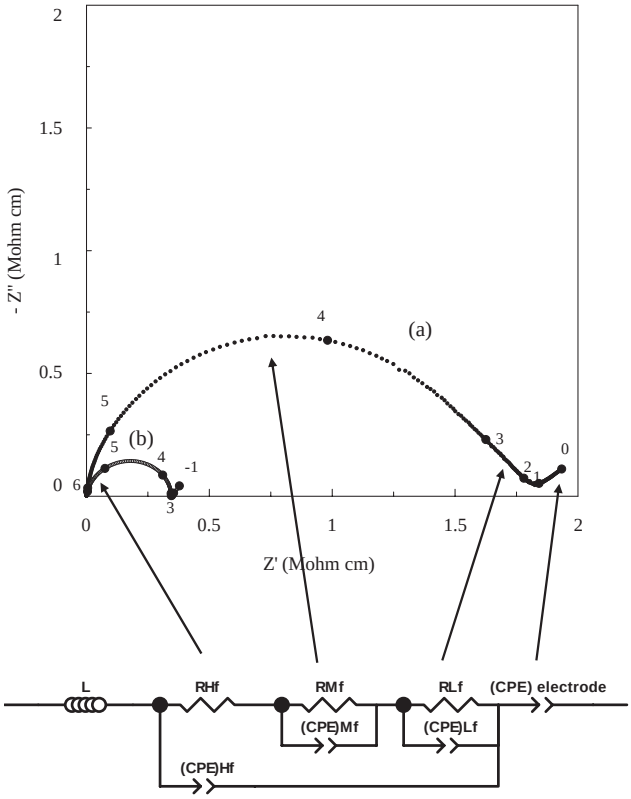

Fig. 7. Normalized impedance spectra, recorded at 200 °C, of $Li_{0.30}Ca_{0.35}TaO_3$ sample obtained by PC route after heating at 1300 °C for 2 h and quenching (a) and obtained by SSR (b) with the equivalent electrical circuit proposed. The normalizing factor is the pellet geometric factor $(S/L)_{pellet}$.

obtained by PC route (1.8 MΩ cm) is much greater than the total resistance of the oxide obtained by SSR (0.35 MΩ cm). This overall behaviour is observed for all the temperature investigated. It is then strongly dependent on the method of preparation and on the microstucture of the oxide. The low frequency part of the diagram, that appears as a straight line, can be attributed to the electrode polarization since the capacity is found to be of the order of 10 μF/cm^2 and increases as temperature increases.

As previously described in [10], the "semicircle" cannot be fitted with only one relaxation. Such an overlapping suggests that bulk and grain boundary relaxation are present in both oxides and that they do not have highly different time constants. We analysed the impedance diagrams by means of an electrical model. From several possible electrical models, made of series or parallel circuits, the model shown in Fig. 7 below the impedance diagram enabled us to fit all the impedance diagrams obtained in the 75–300 °C temperature range, with a weighted sum of squares always smaller than 0.01. The circuit has the same physical origin as the one described in our previous paper dealing with Ca-tantalate obtained by SSR [10]. The diagrams analysis clearly shows that three relaxations are necessary to fit the "semicircle", instead of only two for SSR Ca-tantalate. These three relaxations correspond to three different ionic motions and electrical barriers in the materials. If compared to the oxide prepared by SSR route, the impedance diagram of the oxide obtained by sol–gel route clearly shows two particular features: (i) a low frequency relaxation is added to the impedance diagram (ii) the resistance of the medium frequency relaxation is increased. This would strongly suggest that the blocking effect of the grain boundaries is enhanced when the oxide is prepared by PC route.

The fitting parameters extracted from the equivalent circuit are the resistance, R, and the constant phase element, CPE, of each relaxation. The CPE, which is necessary to take into account that the centre of the semicircle resides below the real axis, is made of a frequency-independent real constant (also named pseudo-capacitance), A, and a constant phase parameter, n. The impedance of the CPE is given by the well-known relationship [15]:

$$Z_{\mathrm{CPE}} = 1/[A(\mathrm{j}\omega)^n], \quad (1)$$

where $\mathrm{j} = \sqrt{1}$, and ω is the angular frequency. Each relaxation is characterized by its own angular relaxation frequency ω_0, which is independent on the geometric factor of the sample. Fig. 8 presents the variation of the characteristic relaxation frequency f_0 ($f_0 = \omega_0/2\pi$) of the three relaxation processes as a function of the inverse of temperature. The three relaxations show a change of the activation energy at 150 °C, as previously

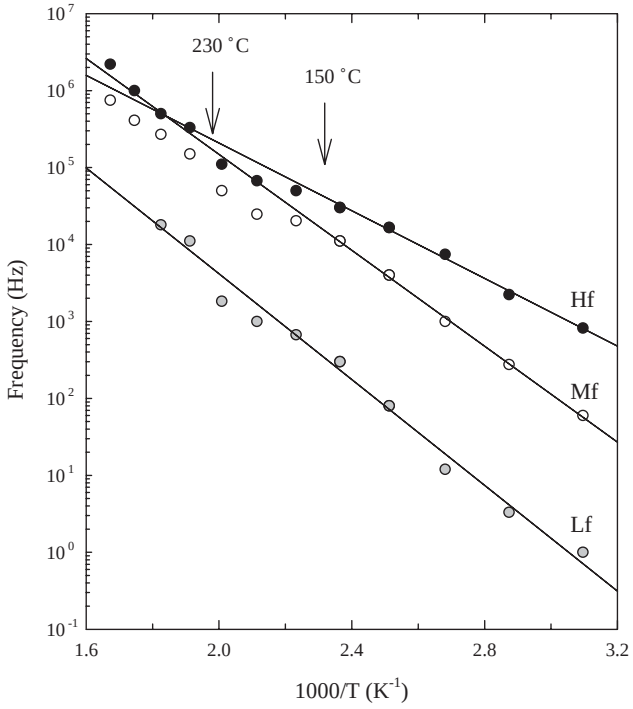

Fig. 8. Variation of the characteristic relaxation frequency f_0 ($f_0 = \omega_0/2\pi$) as a function of inverse of temperature for the three observed relaxations in the high frequency (Hf), the middle frequency (Mf) and the low frequency (Lf) domains.

observed in SSR Ca-tantalate on both the conductance and the NMR spin–lattice relaxation time curves [10]. This suggests, as previously discussed in [10], a change in the mechanism of conduction with temperature. Below 150 °C, the relaxation frequency is thermally activated, in the temperature range from 150 to 230 °C the activation energy decreases and above 230 °C the activation energy increases. This change cannot be ascribed neither to a phase change, as shown by the XRD and thermal analysis data, nor to an irreversible process since the experimental data have been obtained by first increasing the temperature from 125 to 300 °C and then decreasing it to RT.

However we can postulate that a change with temperature in the slight tilting of the TaO_6 octahedra, shown in [9], can yield to some change in the conduction pathways and then in the mechanism of conduction. Neutron diffraction experiments in this range of temperature would be necessary to confirm this assumption. Below 150 °C, the activation energy is 0.44 ± 0.05, 0.62 ± 0.05 and 0.68 ± 0.05 eV for the Hf, Mf and Lf relaxation, respectively.

As described in [15], the resistance and the pseudo-capacitance of a relaxation are related to its angular relaxation frequency ω_0 through the relationship: $\omega_0 = (RA)^{-1/n}$, which is also related to the true capacitance, C, through: $\omega_0 = (\mathrm{RC})^{-1}$. Therefore, it is possible to determine, from the experimental fitting

parameters R, A and n, the true capacitance C of a given relaxation:

$$C = R^{(1-n)/n} A^{1/n}. \quad (2)$$

Figs. 9a and b show the resistance of the three relaxations, obtained from the refinement of the impedance diagrams, and their respective true capacitances, obtained from (2). As expected, the capacitances

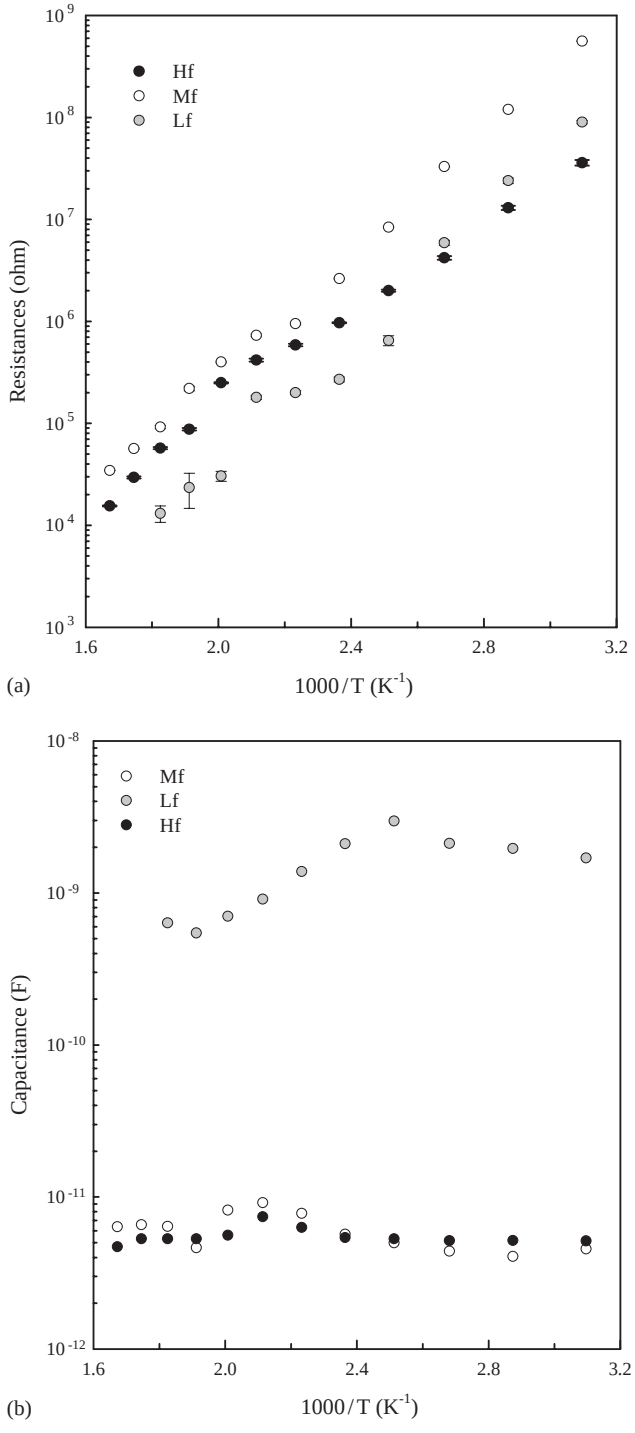

Fig. 9. Variation of the resistance (a) and capacitance (b) as a function of inverse of temperature for the three observed relaxations.

are almost constant with temperature whereas the resistances are thermally activated. A particular behaviour is also observed in these curves between 150 and 230 °C.

The high frequency relaxation (Hf) is ascribed without doubt to the Li^+ motion into the grains of the oxide with the lower activation energy. The medium (Mf) and the low frequency (Lf) relaxations are ascribed to Li^+ motion into the grain boundaries. Two types of grain boundary would then be present in the oxide obtained by the PC method giving rise to two distinct relaxations. This is consistent with the SEM pictures and the laser granulometry analysis, which revealed the presence of small grains of 0.1–0.8 μm size and of aggregates of 8–40 μm. It can then be assumed that two barriers exist, one between the grains inside the aggregates and another one between the aggregates.

The electrical characteristics of the bulk oxide, i.e., the permittivity, $\varepsilon^r_{\text{bulk}}$ and the dc-conductivity, σ_g, can be determined by using the high frequency resistance, R_{Hf}, and the true capacitance, C_{Hf}, with the sample geometry (area S and thickness L) according to the following equations:

$$R_g = R_{\text{Hf}} = \frac{1}{\sigma_g}\left(\frac{L}{S}\right)_{\text{pellet}}, \quad (3)$$

$$C_g = C_{\text{Hf}} = \varepsilon^r_{\text{bulk}}\varepsilon_0\left(\frac{S}{L}\right)_{\text{pellet}}. \quad (4)$$

A permittivity of 55 has been determined, which is in good agreement with previous values of oxides and calcium titanate dielectric constant [16,17]. Fig. 10 shows the bulk dc-conductivity, plotted in an Arrhenius fashion. We also reported in this figure the dc-conductivity previously determined in [10] for the SSR Ca-tantalate. The plots are similar and confirm that the Li^+ conductivity in the grains of these oxides are identical, meaning that the two synthesis routes lead to the same bulk material and modify only the grain boundaries part of the material. The activation energy determined from the plot below 150 °C is found to be 0.43 ± 0.05 eV, the same as the activation energy of the Hf f_0.

To correlate the measured electrical properties with sample microstructure, it is convenient to define a microstructural model. The most widely used model is the simple brick layer model [15,18,19]. Fig. 11 shows a schematic view of the ceramic, drawn with the brick layer model assumption, made of cubic grains of an average size $d_g \approx 0.2$ μm and cubic aggregates, made of n^3 grains, of an average size of $L_{\text{aggregate}} \approx 20$ μm (a). We can assume that the pellet is made of m^3 aggregates (b). According to this scheme, two types of barriers are present, one, of thickness e_1, between the grains and another one, of thickness e_2, between the aggregates.

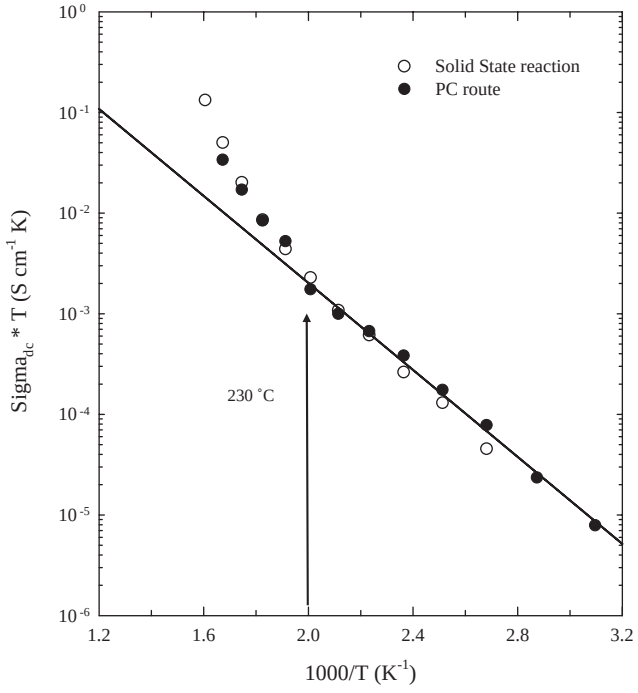

Fig. 10. Bulk dc-conductivity of $Li_{0.30}Ca_{0.35}TaO_3$ sample obtained by PC route after heating at 1300 °C for 2 h and quenching and obtained by SSR.

The form factor of the pellet $(S/L)_{\text{pellet}}$ is then given by:

$$\left(\frac{S}{L}\right)_{\text{pellet}} = mn(d_g + e_1 + \frac{e_2}{n}). \tag{5}$$

As previously mentioned, we can easily assume that $e_1 < d_g$ and that e_2/n is obviously smaller than e_1 since $n > 1$. Therefore, the form factor of the pellet can be approximated to:$(S/L)_{\text{pellet}} = mnd_{\text{g}}$.

To calculate the resistance and capacitance of the grains and the grain boundaries, we assume that electrodes are deposited onto the pellet in the (y,z) planes and that the electric field is then applied along the x-direction, as shown in Fig. 11. According to the brick layer model, the total resistance and capacitance of the pellet due to the grains are:

$$R_{\text{g}} = \frac{1}{\sigma_{\text{g}}}\frac{1}{mnd_{\text{g}}} \tag{6}$$

and

$$C_{\text{g}} = \varepsilon^r_{\text{bulk}}\varepsilon_0 mnd_{\text{g}}. \tag{7}$$

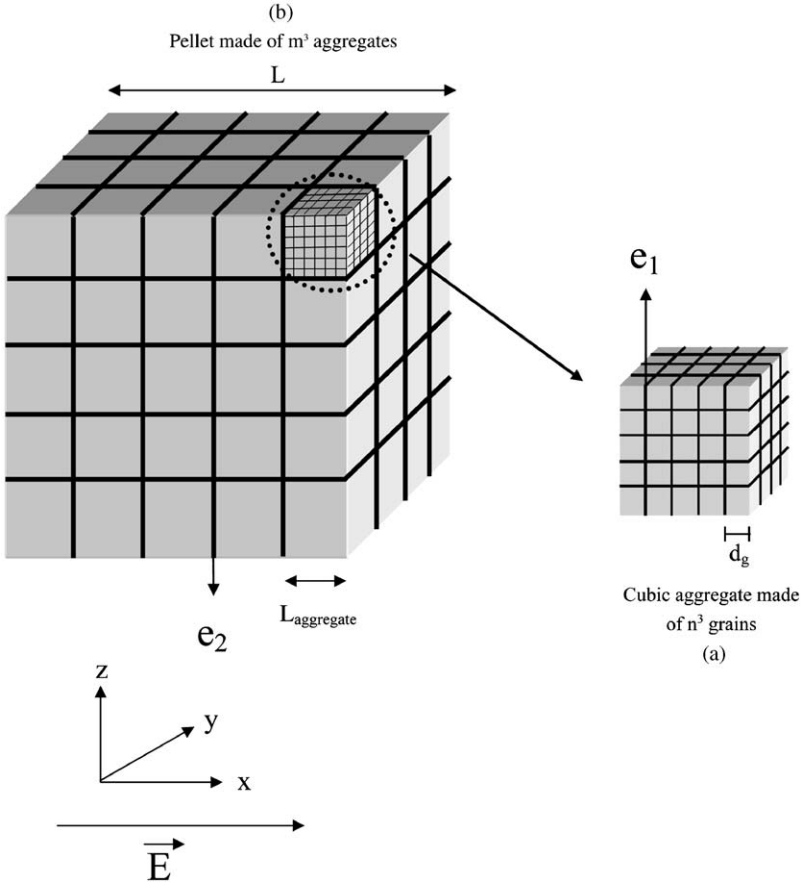

Fig. 11. A schematic view of the ceramic drawn with the brick layer model assumption. We assume that the electrodes are deposited in the (y,z) plane.

The total resistance and capacitance of the pellet due to the grain boundary between the grains are:

$$R_{(gb)1} = \frac{1}{\sigma_{(gb)1}} \frac{e_1}{mn(d_g)^2} \tag{8}$$

and

$$C_{(gb)1} = \varepsilon^r_{(gb)1}\varepsilon_0 \frac{mn(d_g)^2}{e_1} \tag{9}$$

and the corresponding total resistance and capacitance of the pellet due to the grain boundary between the aggregates are given by:

$$R_{(gb)2} = \frac{1}{\sigma_{(gb)2}} \frac{e_2}{mn^2(d_g + e_1)^2} \tag{10}$$

and

$$C_{(gb)2} = \varepsilon^r_{(gb)2}\varepsilon_0 \frac{mn^2(d_g + e_1)^2}{e_2}. \tag{11}$$

According to the relationships (9) and (11), it can be shown that $C_{(gb)2} > C_{(gb)1}$, therefore the Mf capacitance can be ascribed to the grain boundary between the grains, $C_{(gb)1}$, and the Lf capacitance to the grain boundary between the aggregates, $C_{(gb)2}$. Furthermore, Fig. 9b shows that C_g is of the same order of magnitude than $C_{(gb)1}$, i.e., $C_{(gb)1}/C_g \approx 1$. Since the grain boundary thickness e_1 is smaller than the grain size d_g and according to the relationships (7) and (9), the permittivity of the grain boundary between the grains is much smaller than the bulk one and can be approximated to the following relationship:

$$\varepsilon^r_{(gb)1} \approx \varepsilon^r_{bulk} \frac{e_1}{d_g}. \tag{12}$$

Because $\omega_0 = (RC)^{-1}$, the following relationship exists between the permittivity and the electrical conductivity of a particular medium:

$$\sigma_i = \varepsilon^r_i \varepsilon_0 (2\pi f^i_0), \tag{13}$$

where σ_i is the conductivity of the phase i, ε^r_i its permittivity, ε_0 the free space permittivity and $(2\pi f^i_0)$ the angular relaxation frequency. Therefore, the conductivity of grain boundary 1, $\sigma_{(gb)1}$, can be obtained by using the relationships (7), (8) and (9) with $\omega_0 = (RC)^{-1}$ for the grain boundary 1:

$$\sigma_{(gb)1} = \varepsilon^r_{bulk} \left[\frac{e_1}{d_g} \frac{C_{(gb)1}}{C_g}\right] \varepsilon_0 (2\pi f^{Mf}_0). \tag{14}$$

Because the term into brackets is not equal to unity, it is not possible to assume that the permittivity of the grain boundary is the same as the one of the bulk oxide. Microstructural information are then necessary to determine the true grain boundary conductivity. In the same manner, the grain boundary conductivity between the aggregates, $\sigma_{(gb)2}$ can be determined with relationships (9), (10) and (11) with $\omega_0 = (RC)^{-1}$ for the grain boundary 2:

$$\sigma_{(gb)2} = \varepsilon^r_{bulk} \left[\frac{e_1}{L_{aggreg}} \frac{C_{(gb)2}}{C_{(gb)1}}\right] \varepsilon_0 (2\pi f^{Lf}_0). \tag{15}$$

The permittivity and the dc-conductivity of the grain boundaries can than be calculated from the values of the capacitances and the characteristic frequencies f_0. Fig. 12a shows the plot of the permittivity of the bulk and grain boundaries, obtained from (4), (14) and (15), as a function of temperature. Fig. 12b shows the corresponding dc-conductivity as a function of temperature. To determine these values we used the following assumptions: $e_1/d_g = 0.1$ and $e_1/L_{aggreg} = 10^{-3}$. It is observed that the permittivity of the grain boundaries is smaller than the bulk one, indicating that grain boundaries are slightly different in nature than the bulk material. It can

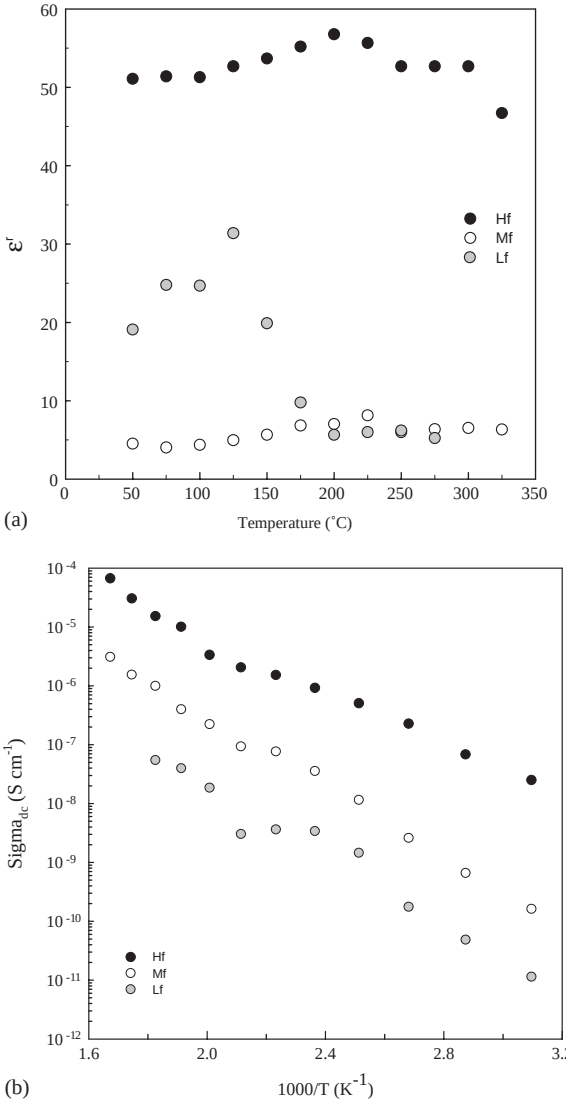

Fig. 12. Variation of the permittivity (a) and dc-conductivity (b) of the bulk (g-Hf), the grain boundary between the grains (gb_1-Mf) and the grain boundary between the aggregates (gb_2-Lf) as a function of temperature.

be postulated that some Li^+ mobile ions may be missing from these grain boundaries. Consequently, the grain boundary dc-conductivity is smaller than the bulk dc-conductivity, indicating that the grain boundaries formed barriers to the ionic motion, as already suggested by the impedance diagrams.

4. Conclusion

The Li^+ ionic conductor, $Li_{0.30}Ca_{0.35}TaO_3$, was synthesized by a Pechini-type polymerizable precursor (PC) method. The method described herein is based on the formation of precursors, which are very stable in open air. The final powder, obtained by heating the powder precursors at 1300 °C for 2 h in air followed by quenching at RT, is a pure and well-crystallized $Li_{0.30}Ca_{0.35}TaO_3$ phase as revealed by powder XRD and TEM. Both synthesis time and synthesis temperature of this oxide are considerably reduced in comparison to the conventional Solid-State Reaction method. Small particles ($<1\,\mu m$) are formed which aggregate in 10–40 μm agglomerates. Despite the low energy consuming way of preparation, this PC synthesis procedure leads to the formation of more blocking grain boundaries that increase the overall impedance of the oxide. The blocking effect is mostly due to the low permittivity of the grain boundaries.

Acknowledgments

We thank Pr. Jean-Louis Fourquet and Yoshiyuki Inaguma, invited Professor of the "Université du Maine" for appreciate discussions in the synthesis procedure. Q.N. Pham thanks the MRT of France for the Ph.D fellowship, M. Vijayakumar thanks the "Région des Pays de la Loire" for postdoctoral fellowship. We also thank M.J.-J. Péchon-Rossel from the Institute of Technology of the "Université du Maine" for the possibility of granulometry measurements.

References

[1] A.G. Belous, V.I. Butko, G.N. Novitskaya, S.V. Polianetskaya, B.S. Khomenko, Y.M. Poplavko, Ukr. Fiz. Zh. 31 (4) (1986) 576.
[2] Y. Inaguma, C. Liquan, M. Itoh, T. Nakamura, T. Uchida, H. Ikuta, M. Wakihara, Solid State Commun. 86 (10) (1993) 689.
[3] C. Bohnké, H. Duroy, J.L. Fourquet, Sensors Actuators B 89 (2003) 240.
[4] C. Bohnké, J.L. Fourquet, Electrochim. Acta 48 (2003) 1869.
[5] K. Mizumoto, S. Hayashi, J. Ceram. Soc. Jpn. 105 (8) (1997) 713.
[6] K. Mizumoto, S. Hayashi, Solid State Ionics 116 (1999) 263.
[7] K. Mizumoto, S. Hayashi, Solid State Ionics 127 (2000) 241.
[8] C.Y. Sun, K.Z. Fung, Solid State Commun. 123 (2002) 431.
[9] Q.N. Pham, M.P. Crosnier-Lopez, F. Le Berre, F. Fauth, J.L. Fourquet, Solid State Sci. 6 (9) (2004) 923.
[10] Q.N. Pham, C. Bohnké, J. Emery, O. Bohnké, F. Le Berre, M.P. Crosnier-Lopez, J.L. Fourquet, P. Florant, Solid State Ionics 176 (2005) 495–504.
[11] US Patent 3,330,697, 1967.
[12] J. Szanics, T. Okubo, M. Kakihana, J. Alloys Compds. 281 (1998) 206–210.
[13] (a) J. Rodriguez Carjaval, FULLPROF program; Rietveld Pattern Matching Analysis of Powder Patterns, ILL, Grenoble, 1990;
(b) H.M. Rietveld, J. Appl. Crystallogr. 2 (1969) 65.
[14] J.R. Macdonald, Solid State Ionics 58 (1992) 97–107.
[15] J.R. Macdonald, Impedance Spectroscopy, Wiley, New-York, 1987.
[16] O. Bohnké, J.C. Badot, J. Emery, J. Phys.: Condens. Matter 15 (2003) 7571–7584.
[17] E. Chinaro, J.R. Jurado, F.M. Figueiredo, J.R. Frade, Solid State Ionics 160 (2003) 161–168.
[18] T. van Dick, A.J. Burggraaf, Phys. Stat. Sol. A 63 (1981) 229.
[19] M.J. Verkerk, B.J. Middelhuis, A.J. Burggraaf, Solid State Ionics 6 (1982) 159.